Mineralogy and Petrology (1995) 55: 1–26

Mineralogy and Petrology

Mineralogical and geochemical evolution of micas from miarolitic pegmatites of the anorogenic Pikes Peak batholith, Colorado

E. E. Foord[1], P. Černý[2], L. L. Jackson[3], D. M. Sherman[4], and R. K. Eby[5]

[1] Branch of Central Mineral Resources, U.S. Geological Survey, Denver, USA
[2] Department of Geological Sciences, University of Manitoba, Winnipeg, Canada
[3] Branch of Geochemistry, U.S. Geological Survey, Denver, USA
[4] Branch of Geophysics, U.S. Geological Survey, Denver, USA
[5] Topometric, Bedminister, USA

With 12 Figures

Received December 27, 1993;
accepted January 12, 1995

Summary

A suite of 29 micas from miarolitic pegmatites associated with granitic units of the anorogenic Pikes Peak batholith (1.08–1.02 Ga), Colorado range in composition, and follow in paragenetic sequence, from 1M siderophyllite (N = 1), and 3T or $2M_1$ lithian biotite (N = 5) to 1M zinnwaldite (N = 20) and 1M ferroan lepidolite (N = 1). Locally, 1M (?) phlogopite (N = 1) and ferroan $2M_1$ muscovite (N = 1) are also present. Pervasive, late-stage hydrothermal alteration along with possible supergene weathering of many of these micas produced vermiculite. Additionally, some vugs and cavities were filled with chlorite and/or smectite. Early crystallized micas form tapered columnar crystals in graphic pegmatite, growing toward, and adjacent to the miarolitic cavity zone which contains the later crystallized micas. Principal associated minerals are quartz, microcline perthite (mostly amazonite), and albite, with local topaz or fluorite, and rarely tourmaline (schorl-elbaite).

Progressively younger micas of the main crystallization sequence display increasing Si, Li, F, and Al/Ga, and decreasing total Fe, Mg, and octahedral occupancy. The zinc content of all micas is considerably elevated, whereas Mn, Rb, Cs, and Sc are moderate and Tl is very low. Early siderophyllite and lithian biotite show a narrow range of FeO/Fe_2O_3 (5.6–8.0), whereas later zinnwaldite is much more variable (2.4–40.3). Annite of the host granite and early graphic pegmatite is compositionally homogeneous, but most mica crystals from cavities show remarkable compositional and abrupt, sharp and distinct color zoning. Most cavity-grown zinnwaldite crystals show a decrease, from core to rim, in total Fe and Mg, whereas Si, Li and F increase and Mn, Rb, Cs and Na are essentially constant. A few to more than 100 color zones have been identified in some mica crystals.

The zones are well correlated with the Ti content (<0.2 wt. % TiO_2 colorless, 0.4–0.6 wt.% TiO_2 red-brown). The total Fe content may or may not correlate with color zoning, whereas Zn variations (up to 1.1 wt. %) are entirely independent. The dark color zones probably reflect Fe-Ti charge transfer.

The mica composition sequence described here is typical of the extreme fractionation observed in pegmatites of the NYF family, associated with anorogenic granites. Elevated Fe, Zn, and enhanced Sc contents are characteristic of this family. Strong enrichment in Li, Rb, and F is present, particularly in the micas of the miarolitic cavities. Sharp color zonation and compositional variation in cavity-grown zinnwaldite and ferroan lepidolite crystals suggest rapid changes in the intensive parameters, particularly the $f(O_2)$, of the parent fluid during the final stages of pegmatite consolidation

Zusammenfassung

Glimmer aus dem Pikes Peak Batholith, Colorado

29 Glimmer aus miarolithischen Pegmatiten, die mit den Graniten des anorogenen Pikes Peak Batholiten (1.08–1.02 Ga) in Colorado vorkommen, schwanken in ihrer Zusammensetzung, und folgen in paragenetischer Abfolge, von 1M Siderophylit (N = 1) und 3T oder $2M_1$ Lithium Biotit (N = 5) bis zu 1M Zinnwaldit (N = 20) und 1M Eisen-Lepidolit (N = 1). Lokal kommt auch 1M (?) Phlogopit (N = 1) und $2M_1$ Eisen-Muskovit (N = 1) vor. Anhaltende hydrothermale Umwandlung während später Stadien der granitischen Entwicklung und möglicherweise auch oberflächennahe Verwitterung mancher dieser Glimmer führte zur Entstehung von Vermiculit. Außerdem wurden einzelne Hohlräume mit Chlorit und/oder Smectit gefüllt. Die früh gebildeten Glimmer sind säulige Kristalle in graphischem Pegmatit, die in Richtung auf, und in Nähe der blockigen Zone wachsen; der Großteil der später gebildeten Glimmer ist in der blockigen Zone und in an diese anschließenden miarolithischen Hohlräumen lokalisiert. Die wichtigsten assoziierten Minerale sind Quarz, Mikroklin-Perthit (hauptsächlich Amazonit), sowie Albit, mit lokal etwas Topas oder Fluorit, und selten Turmalin (Schörl-Elbait).

Die Hauptabfolge der Glimmer-Kristallisation zeigt zunehmende Si, Li, F und Al/Ga, aber abnehmende Gesamtwerte für Fe, Mg, und oktaedrische Besetzung. Der Zinkgehalt ist beträchtlich erhöht, während Mn, Rb, Cs, und Sc mittlere und Tl sehr niedrige Werte zeigen. Frühgebildete Siderophylite und Lithium-Biotite zeigen beschränkt Variationen der FeO/Fe_2O_3 Verhältnisse (5.6–8.0), während späterer Zinnwaldit mehr variabel ist (2.4–40.3). Annit im Wirts-Granit und in frühem graphischen Pegmatit ist seiner Zusammensetzung nach homogen, aber die meisten Glimmerkristalle aus Hohlräumen zeigen bemerkenswerte Zonierung der Zusammensetzung und gut entwickelte Farb-Zonierung. Die meisten in Hohlräumen gewachsenen Zinnwaldit-Kristalle zeigen eine Abnahme an Fe und Mg von Kern zum Rand, während Si, Li, und F zunehmen, sowie Mn, Rb, Cs und Na konstant bleiben. Es können einige wenige, aber auch mehr als 100 Farbzonen entwickelt sein, und diese sind gut mit dem Ti-Gehalt (<0.2 Gew. % TiO_2 farblos, 0.4–0.6 Gew. % TiO_2 rot-braun) zu korrelieren. Der Gesamteisengehalt kann, aber muß nicht mit der Farb-Zonierung korrelierbar sein, während Variationen des Zinkgehaltes (bis zu 1.1 Gew %) vollkommen unabhängig von optischen Aspekten sind. Das Auftreten tieferer Farbtöne dürfte einem Fe-Ti Ladungstransfer zuzuschreiben sein.

Die hier diskutierte Abfolge von Glimmern ist typisch für extreme Fraktionierung in Pegmatiten der NYF Familie, die mit anorogenen Graniten assoziiert sind. Hohe Gehalte von Fe, Zn und erhöhte Sc Gehalte sind charakteristisch. Deutliche Anreicherung an Li, Rb und F ist besonders in den Glimmern aus miarolithischen

Hohlräumen festzustellen. Der gut entwickelte optische und chemische Zonenbau in Zinnwaldit und Eisen-Lepidolith Kristallen, die in Hohlräumen gewachsen sind, weist auf intensiven Wechsel der intensiven Parameter der Mineral-bildenden Fuide in den Endstadien der Pegmatit-Bildung hin; dies trifft besonders auf $f(O_2)$ zu.

Introduction and previous studies

This study of micas from the miarolitic pegmatites of the Pikes Peak batholith (PPB) and slightly younger cogenetic sodic and potassic plutons was undertaken to provide information on the geochemical evolution and paragenesis of the micas and the pegmatites themselves. In general, very few compositional studies of micas from pegmatites of anorogenic igneous suites are available; and most of these are outdated. It was also desirable to compare the Fe-Li micas (i.e. siderophyllite, zinnwaldite and lepidolite) from pegmatites in anorogenic granitoids with those of micas from granitoids in other geologic environments (peraluminous pegmatites, greisens, veins, granites, e.g. in recent studies such as those of *Henderson* et al., 1989; *Černý* et al., 1993; *du Bray,* 1994). More specifically, modern mineralogic and chemical studies are lacking for the micas in pegmatites associated with the PPB. A suite of 30 samples of lithian biotite, siderophyllite, zinnwaldite, ferroan lepidolite (polylithionite), muscovite, phlogopite and one vermiculite sample pseudomorphous after zinnwaldite were chemically characterized. Polytypism was determined for 22 samples. The chemical and structural variations in the micas representing progressive crystallization and culminating with those in closed-system miarolitic cavities are of particular interest in characterizing the final stage of cogenetic granite-pegmatite crystallization.

Detailed studies of micas from the PPB are scarce (e.g. *Gross* and *Heinrich,* 1965; *Puffer,* 1972; *Barker* et al., 1975; *Hawley* and *Wobus,* 1977; *Desborough* et al., 1980). All of these studies document the composition of micas from various granitic units of the batholith. Annite, indicative of the iron enrichment characteristic of the PPB, occurs in the Lone Rock pluton (formerly known as the Rosalie lobe) and in the Pine area (South Platte District) (unpublished data from *David Frishman* and *Warren Day,* USGS, 1993). A detailed Mössbauer spectral study of one annite from the Devil's Slide, near Mount Rosa, was made by *Dyar* and *Burns* (1986). Siderophyllite from Pikes Peak was defined as a new species by *Lewis* (1880). A zoned iron-rich mica from near Pikes Peak was studied by *Clark* (1887). From *Clark*'s analyses, it appears that a core of vermiculite is surrounded by partly altered and oxidized ferrian biotite.

Many of the studies of micas, including Li-Fe micas, from granitic pegmatites have been summarized by *Černý* and *Burt* (1984). Among the more recent additions to the studies of micas from pegmatites, the study of zoned zinnwaldite-masutomilite crystals from pegmatites in the Sawtooth batholith, Idaho described by *Menzies* and *Boggs* (1993); composition trends for micas from the Bob Ingersoll pegmatite, Black Hills, South Dakota (*Jolliff* et al., 1987); a study of aluminous micas from pegmatites by *Gordiyenko* et al. (1991); the physico-chemical conditions of formation of lepidolite by *Ponomareva* and *Gordiyenko* (1991); a study of mica evolution in pegmatites of the Czech Republic by *Černý* et al. (1995) and a study of biotites from rare-element granitic pegmatites in the Grenville Province, Canada (*Lentz,* 1992) are recent sources of information on micas from pegmatitic systems.

Geologic setting

Proterozoic metavolcanic and metasedimentary rocks in the Front Range of Colorado were invaded by granitic anorogenic plutons during three major intrusive episodes at about 1.7, 1.4 and 1.1 Ga respectively. The plutons were emplaced at successively shallower crustal levels during the gradual uplift of the regions (*Wobus* and *Hutchinson,* 1988). The emplacement of the PPB and its associated stocks occurred during the last intrusive episode of plutons composing the PPB (1.1 Ga, U-Pb age for zircon, *Schärer* and *Allégre,* 1982). Emplacement of plutons composing the PPB is estimated to have occurred during a 20–50 m.y. interval as indicated by U-Pb zircon and Ar^{40}/Ar^{39} amphibole ages (*Daniel Unruh* and *Lawrence Snee,* USGS, pers. commun., 1993). Rb-Sr and K-Ca dates are 50 to 80 m.y. younger because feldspars remained open to diffusion well after emplacement (*Blasi* et al., 1984). Shallow (epizonal) emplacement is supported by the mineralogical studies of *Barker* et al. (1975), *Foord* and *Martin* (1979), and *Blasi* et al. (1984). A single ε_{Nd} determination for a syenite specimen suggests that the PPB is "the end product of a complex magmatic history of crystallization and crustal assimilation, beginning with a mantle-derived basaltic magma" (*DePaolo,* 1981). It should be remembered that at the pocket stage of pegmatitic evolution, we are studying the final products of crystallization of a very evolved granitic magma.

Pegmatites generated by fractionation of the Pikes Peak batholith granites are typical representatives of the NYF family, enriched in Nb > Ta,Ti,Y,Sc,REE, Zr,U, Th and F (*Černý,* 1991a,b,c). Two categories can be distinguished: (1) the relatively deep-seated pegmatites of the rare-element class, rare-earth type (found in the northern part of the batholith; *Simmons* et al., 1987; *Černý,* 1992), and (2) the relatively shallow-seated to subvolcanic pegmatites of the miarolitic class. Micas in the latter category of pegmatites are the subject of our present study. These pegmatites, and their cavity assemblages, are the final products of extended differentiation of granitic magma which reached very high levels of geochemical evolution.

Samples examined

Samples studied in detail come from four areas: (1) Lake George ring structure, 16 samples, (2) Wigwam Creek area, 12 samples, (3) Devils Head, 1 sample, and (4) Harris Park, 1 sample. Additional samples of zinnwaldite from a large pegmatite pocket found in 1990 near Harris Park were also studied but not completely analyzed. Figure 1 is a simplified geologic map of the southern Front Range showing the four areas. Sample descriptions and mineral associations are given in Table 1. The sampling is not as systematic or complete as would be desirable, mainly because of the relative scarcity of pocket micas, and because most micas whose compositions would be of some interest, in the clay- and iron-maganese oxide-filled cavities as well as the graphic and blocky zones of pegmatite bodies are hydrothermally and/or surficially weathered (conversion to vermiculite) and therefore unsuitable for analysis. The 'dispersed' sampling, done principally by others, undoubtedly affects our attempts to define geochemical evolution trends, but probably is sufficient to identify all mica varieties in the examined pegmatites.

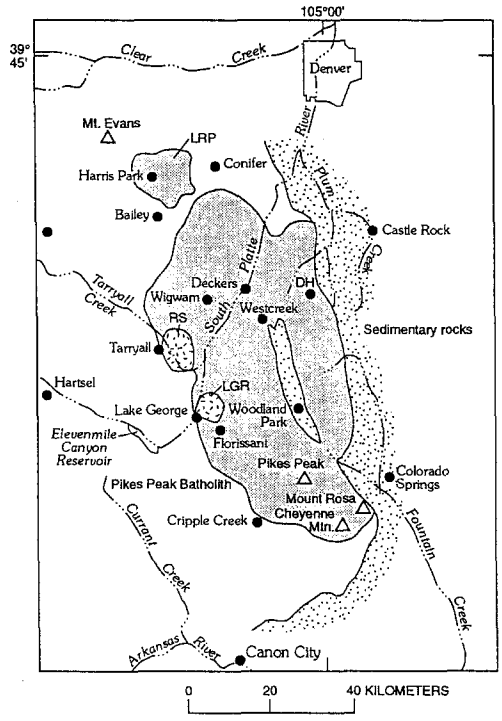

Fig. 1. Simplified geologic map of the Colorado Front Range showing the Pikes Peak batholith (PPB) and sample locations. Stippled area – sedimentary rock cover, hachured area – PPB, dashed area – late potassic-sodic plutons. *LRP* Lone Rock pluton, *RS* Redskin stock, *LGR* Lake George ring, *DH* Devils Head

Table 1. *Description of mica samples from pegmatites of the Pikes Peak batholith*

Sample No.	Sample description and associated minerals
1a	light brown core portion of color-zoned zinnwaldite crystal from miarolitic cavity near Wigwam Creek. Associated with medium blue amazonite, albite, fluorite and smoky quartz.
1b	dark brown rim portion of color-zoned zinnwaldite crystal from Wigwam Creek.
2	blue-green to green lithian biotite crystal from graphic quartz-K-feldspar pegmatite adjacent to miarolitic cavity. Lake George ring (LGR).
3	bright blue green lithian biotite crystal from graphic quartz-K-feldspar pegmatite adjacent to a miarolitic cavity. From a different pegmatite body 20 m away from no. 2.
4	pale brown lithium-iron-bearing muscovite from miarolitic cavity near Crystal Peak, LGR. Associated with quartz, K-feldspar, albite.
5	tapered dark brown phlogopite from graphic pegmatite adjacent to miarolitic cavity. From same location as nos. 2 and 3.
8	medium brown zinnwaldite from miarolitic cavity near Crystal Peak, Lake George Ring. Associated with quartz, and pale blue amazonite.
9	medium brown zinnwaldite from miarolitic cavity N W of Crystal Peak, LGR. Associated with quartz, and pale blue amazonite with minor albite.
86-25	pale tan zinnwaldite from quartz core zone of a pegmatite on Goethite Hill, LGR. Associated with quartz, buff-tan to pink K-feldspar and very pale amazonite, with minor albite.

(*Continued*)

Table 1. (*Continued*)

Sample No.	Sample description and associated minerals
86-26	pale tan zinnwaldite from miarolitic cavity. Associated minerals are quartz, K-feldspar, albite and purple fluorite. LGR.
86-27	medium tan-brown zinnwaldite from miarolitic cavity at Wigwam Creek. Associated with quartz, K-feldspar, albite and topaz.
21	very pale brown ferroan lepidolite from miarolitic cavity NW of Crystal Peak, LGR. Associated with pale to medium blue amazonite with flesh-cream overgrowth on all faces, quartz, and albite.
22	pale brown zinnwaldite from miarolitic cavity W of Crystal Peak, LGR. Associated with quartz, medium blue-green amazonite, and minor albite.
23	Pale brown zinnwaldite from miarolitic cavity near Harris Park. Associated with blue amazonite, smoky quartz, and albite.
24-1	pale brown zinnwaldite from miarolitic cavity near Wigwam Creek. Crystal is not color-zoned. Associated with pale blue amazonite, smoky quartz and albite.
24-2a	rim portion of a pale brown color-zoned crystal of zinnwaldite from a miarolitic cavity near Wigwam Creek. Associated with pale amazonite, quartz, and albite.
24-2b	core portion of crystal 24-2a.
25-a	outermost zone of a medium to dark brown color-zoned crystal of zinnwaldite from a miarolitic cavity near Wigwam Creek. Associated with pale blue-green amazonite, topaz, quartz, albite, and minor schorl-elbaite.
25-b	intermediate zone of same crystal.
25-c	core portion of same crystal. Not color-zoned.
26	vivid green lithian biotite crystal from a quartz core in a pegmatite near Wigwam Creek. Associated with quartz, buff-tan to pink K-feldspar, and minor albite.
27	pale brown zinnwaldite from miarolitic cavity on north side of Trail Creek Rd, LGR. Associated with amazonite, smoky quartz, and minor albite.
41	brown zinnwaldite from a miarolitic cavity near Virgin's bath, Devils Head. Associated with smoky quartz, cream-colored K-feldspar, albite and topaz.
42	very dark brown annitic siderophyllite crystal from a quartz core in pegmatite at Cedar Mtn. no. 1 mine, LGR. Associated with quartz, white microcline, albite and minor zircon.
43	medium brown zinnwaldite from quartz core in pegmatite near Wigwam Creek. Associated with medium to deep blue-green amazonite, quartz and albite.
44	bronze-colored vermiculite pseudomorph after pseudohexagonal 'barrel' of zinnwaldite from edge of a miarolitic cavity near Hackett Gulch, LGR. Associated with pale blue-green amazonite, quartz, and minor albite.
45	medium green lithian biotite from a quartz core in pegmatite near Crystal Peak, LGR. Associated with quartz, medium blue-green amazonite, and albite.
46	medium brown zinnwaldite crystal from quartz core in pegmatite near Wigwam Creek. Associated with medium to deep blue amazonite, quartz and some albite.
47	greenish brown 'barrel' of lithian biotite from quartz and K-feldspar rich core of a pegmatite near Crystal Creek, LGR. Associated with medium-deep blue green amazonite, quartz, and albite.
48	pseudohexagonal 'barrel' of medium brown zinnwaldite from miarolitic cavity near Crystal Creek, LGR. Associated with medium blue amazonite, smoky quartz, and minor albite.

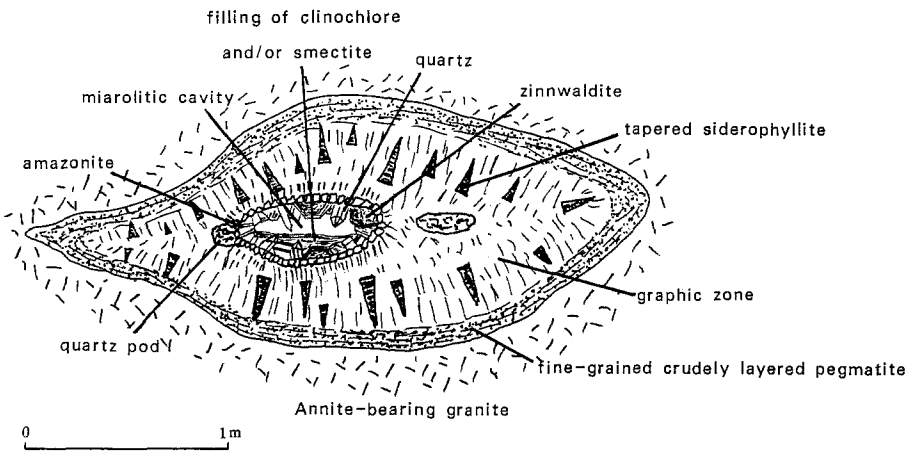

Fig. 2. Schematic cross-section through a typical pegmatite containing a miarolitic cavity

Phlogopite, and siderophyllite form tapered crystals in graphic pegmatite growing toward, and adjacent to, the miarolitic cavity zone; all other micas are from immediately adjacent to and from within miarolitic cavities (Fig. 2). Principal cogenetic minerals are quartz, microcline perhite (mostly of the amazonite variety) and albite, with local topaz or fluorite, and rarely tourmaline of the schorl-elbaite series. Significant compositional and distinct, sharp color zoning, resulting from primary growth fluctuations, are present in most mica crystals formed in miarolitic cavities (Figs. 3a and b). A few to more than 100 distinct zones are developed. However, biotite (annite) in the host granite and early graphic pegmatite is compositionally homogeneous (*Barker* et al., 1975; *Hawley* and *Wobus,* 1977).

Instrumentation and methods

Electron microprobe analyses were made using an ARL SEMQ instrument equipped with 6 wavelength dispersive crystal spectrometers. A two-micron beam and a 15 kV accelerating voltage with 10 nA sample current were used to make multiple analyses (generally five) on individual crystals. Analysed natural and synthetic minerals were used as standards; all data was reduced using MAGIC IV (*Colby,* 1968).

Most of the chemical analyses were done at the Laboratoire de Géochimie Analytique, Ecole Polytechnique, Montreal, Canada (V.J. Kubat): SiO_2, Al_2O_3, total Fe by X-ray fluorescence spectrometry, Tl_2O by a modification of the method of *Fratta* (1974), and Ga_2O_3 by XRF spectrometry of cupferron precipitates (cf. *Černý* and *London,* 1983 for details). All other metals were determined by atomic absorption spectrophotometry. Some of the mica samples were also examined and analyzed with a Cambridge Stereoscan 250 Mk2 scanning electron microscope with EDS capability utilizing Tracor Northern software. For some of the samples, chemical analyses for major oxides were done using XRF techniques at the U.S. Geological Survey. Cl and F were determined in most samples by ion-selective electrode techniques. Water (plus and minus) for most samples was determined using

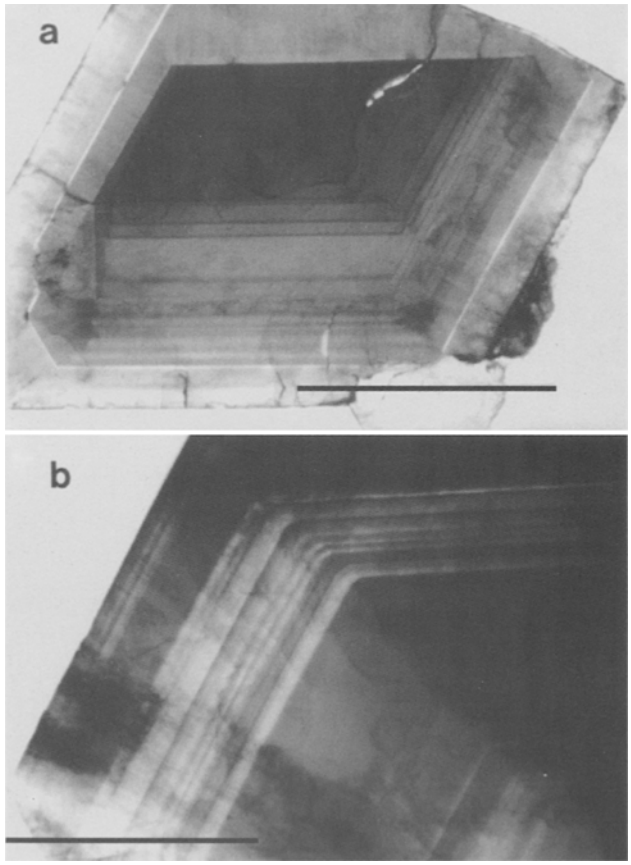

Fig. 3. **a** Zoned crystal of zinnwaldite (samples 1a and 1b) from Wigwam Creek, CO. Note the presence of sharp, multiple growth zones in various shades of red brown to yellow, principally caused by variations in TiO_2 content. Scale bar equals 1 cm. **b** Zoned crystal of zinnwaldite (#46) from Wigwam Creek showing alternation of medium tan and colorless zones. Scale bar equals 1 cm

coulometric Karl-Fisher titration at the USGS (Denver). ICP-AES analyses for 40 major, minor and trace elements also were done on three samples at the USGS. X-ray diffraction studies were performed at the University of Manitoba using the procedure outlined by *Bailey* (1984) for determination of polytypes (for most cases the 00*l* and 0*kl* diffraction maxima on precession photographs). Ferrous-ferric iron ratios were determined by wet chemistry for all except three samples (*W. Blonsky*), and by Mössbauer spectroscopy on nine samples at the USGS. Partial INAA analyses of twelve samples performed at the Univ. of Michigan were provided by *W. B. Simmons* (Univ. of New Orleans-Lakefront). Cation proportions in mineral structural formulas were calculated from major oxide data using the method of *Foster* (1960a,b); anion proportions were calculated separately using the method of *Deer* et al. (1966, p. 515–517). This approach to calculation of atomic contents and their structural allocation is rather simplistic but sufficient to provide a uniform basis for mutual comparison of the different mica samples and species. The emphasis of our study is on geochemistry and evolution trends, not on the fine points of crystal chemistry. Additional chemical-analytical and X-ray diffraction studies would be required to check for interlayer Li^+ (e.g. *Robert* et al., 1983), interlayer H_2O, H_3O^+

or both (*Loucks*, 1991), or tetrahedral Fe^{3+} (*Rancourt* et al., 1992), but they were beyond the scope of our work.

Results

Chemical composition

Chemical compositions for thirty samples were obtained, four samples were not analyzed for water because of insufficient sample. Fourteen of the thirty samples have only total water determined rather than both plus and minus water. For those samples, a value of 0.3 wt. % H_2O^- was assumed on the basis of the other water determinations. Five of the thirty samples have only total Fe determined because of insufficient sample. The FeO/Fe_2O_3 (oxide) ratio was set at 6.0 for those samples, by analogy with the average of comparable samples from our sample suite. Cl was determined for thirteen of the samples. The highest value determined was 0.1 wt %; these results suggest that all Cl abundances are very minor or absent. Table 2 shows the chemical compositions for all of the micas analyzed, polytypes, species designation, and includes explanatory comments where appropriate. Table 3 contains calculated empirical formulas for each of the micas. The nomenclature classification of *Stone* et al. (1988) is used in this paper.

Besides Si and Al, P (present in only minor amounts) is the only other element assigned to the tetrahedral site. Tetrahedral occupancies of Si for the various micas are: muscovite, 6.03, phlogopite 5.81, siderophyllite 6.07, lithian biotite 5.62 to 6.53, zinnwaldites 6.25 to 6.71, and ferroan lepidolite 6.90. The large range (nearly one atom of Si) for the five samples of lithian biotite may reflect changes in the activity of Si and/or Al in the closed pegmatite system.

Octahedral site occupancy (Fig. 4a) for the ferroan-lithian muscovite is 4.3 rather than the ideal 4.0 *a.p.f.u.* The composition of the muscovite (#4) plots between, not along, either of the lithium mica compositional trends, identified by *Foster* (1960a,b). Consequently, as stated by *du Bray* (1994) for a similar muscovite from Saudi Arabia, this muscovite may be a mixed-layer form, involving both dioctahedral and trioctahedral structures, and may represent disequilibrium crystallization. *Monier* and *Robert* (1986) have discussed the evolution of the miscibility gap between biotite and muscovite solid solution with increasing Li content and concomitant increasing F content. Octahedral occupancies (Fig. 4a) for the lithian biotites (five samples) are between 4.8 and 5.3; those of zinnwaldite are between 5.0 and 6.0, and that of the ferroan lepidolite is 6.0. The occupancies for the single sample of siderophyllite (#42) and phlogopite (#5) are 5.4 and 5.55 respectively. All of these are trioctahedral micas.

Calculated anion site occupancies are approximately 4.0 for most samples, but some are higher or lower. Seventeen of twenty-nine samples have occupancies greater than 4.0 and the additional OH may be indicative of hydronium, $(H_3O)^+$ in the interlayer sites (*Rieder*, 1970; *Loucks*, 1991). Some Li may also be in the interlayer positions rather than all being in the octahedral sheets. Interlayer occupancies are all 2.00 ± 0.07. Two samples (#46,47) have higher and significantly elevated contents of Ca compared to all of the others. This is most likely due to inclusions of fluorite that could not be quantified for a meaningful correction, as was the case for sample #86-26. Eight samples have anion site occupancies less than 4.0.

Table 2. *Chemical compositions for Li-Fe micas from miarolitic pegmatites of the Pikes Peak batholith*

Wt. %	1a	1b	2	3	4	5	8	9	86-25	86-26	86-26*	86-27	21	22	23#	24-1
SiO_2	45.39	47.22	39.15	39.25	44.87	38.88	47.85	43.88	44.2	41.8	42.67	45.7	48.06	44.16	44.41	43.63
TiO_2	0.37	0.17	0.14	0.18	0.16	2.73	0.16	0.21	<0.02	0.05	0.05	0.12	0.10	0.33	0.14	0.08
Al_2O_3	20.39	19.43	19.40	19.35	32.01	15.38	21.03	22.28	20.5	20.8	21.23	19.9	17.67	19.72	17.80	20.22
Fe_2O_3	1.17	1.08	2.63	2.42	0.66	4.43	1.34	2.02	1.32	0.66	0.67	1.75	0.59	0.34	2.00	0.87
FeO	12.24	9.04	18.88	19.48	3.60	14.43	9.92	12.72	13.12	11.28	11.51	11.56	8.10	13.69	11.97	12.31
MnO	0.95	0.78	1.22	0.91	0.75	0.89	0.87	0.90	1.21	4.06	4.14	1.62	0.88	0.53	1.29	2.03
ZnO	0.20	0.20	---	---	---	---	---	---	0.11	0.24	0.24	0.15	0.12	0.15	0.13	0.15
MgO	0.33	0.21	0.50	0.71	0.15	10.18	0.51	0.39	0.11	<0.10	<0.10	0.14	0.09	0.18	0.07	0.02
CaO	0.09	0.07	0.10	0.09	0.07	0.10	0.09	0.08	0.04	1.35	0.10+	0.33	0.11	0.09	0.10	0.12
Li_2O	3.49	4.22	1.00	1.07	1.09	0.06	2.57	2.54	3.23	3.01	3.07	3.00	5.08	2.69	3.81	2.74
Na_2O	0.23	0.31	0.43	0.56	0.56	0.57	0.37	0.25	0.16	0.22	0.22	0.19	0.17	0.14	0.11	0.33
K_2O	10.14	10.37	9.64	9.61	10.34	9.77	10.54	10.18	10.2	9.46	9.66	9.68	10.55	10.28	10.23	9.73
Rb_2O	0.63	0.59	0.65	0.65	0.56	0.14	0.37	0.56	0.28	0.84	0.86	0.68	0.44	0.52	0.48	0.92
Cs_2O	0.03	0.03	0.02	0.02	0.11	0.02	0.11	0.05	0.02	0.03	0.03	0.05	0.04	0.08	0.05	0.025
P_2O_5	<0.1	<0.1	---	---	---	---	---	---	<0.05	<0.05	<0.05	<0.02	0.08	0.09	0.08	0.09
H_2O	0.22	0.43	0.38	0.22	0.13	0.40	0.34	0.18	0.3*	0.3*	0.32	0.05	0.30*	0.30*	---	0.30*
H_2O^+	0.92	1.15	2.78	2.95	4.17	2.75	1.45	1.80	1.18	0.74	0.76	0.66	2.18	1.77	---	1.78
F	6.37	6.61	4.43	4.21	2.53	1.48	7.53	4.94	7.54	8.06	7.37+	7.61	8.26	6.82	7.48	7.29
Cl	---	---	---	---	---	---	---	---	---	---	---	---	<0.01	<0.01	---	<0.01
subtotal	103.16	101.91	101.35	101.68	101.76	102.21	105.05	102.98	103.52	102.90	102.90	103.38	102.82	101.88	100.15	102.635
-O=F+Cl	2.68	2.78	1.87	1.77	1.07	0.62	3.17	2.08	3.17	3.39	3.10	3.20	3.48	2.87	3.15	3.07
Total	100.48	99.13	99.48	99.91	100.69	101.59	101.88	100.90	100.24	99.51	99.80	100.18	99.34	99.01	97.0	99.565
Ba, ppm	23	24	30	35	18	51	17	22	260	6	6	34	82	280	60	18
Sr, ppm	31	25	30	31	13	26	25	34	25	70	70	34	6	5	15	11
Tl_2O, ppm	7.2	5.2	11.1	10.7	16.5	4.3	8.3	6.4	---	---	---	---	7	9	12	15
Ga_2O_3, ppm	102	69	714	644	470	107	274	275	54	215	215	108	55	141	86	249
BeO, ppm	216	189	44	42	64	4	130	97	92	72	72	125	202	123	155	64
Polytype	1M	1M	3T	3T	$2M_1$	1M?	1M	1M	---	---	---	---	1M	1M	1M	1M
Name	Zin.	Zin.	PL	PL	Ms.	Phl.	Zin.	Zin.	Zin.	Zin.	Zin.	Zin.	Lpd.	Zin.	Zin.	Zin.

Table 2. (*Continued*)

Wt. %	24-2a	24-2b	25-A	25-B#	25-C*	26	27	41	42	43#	45	46	47	48#
SiO_2	47.62	44.02	43.12	44.25	43.38	35.76	43.95	42.39	37.14	42.89	38.25	42.51	42.97	42.78
TiO_2	0.01	0.01	0.17	0.07	0.16	0.38	0.21	0.07	1.24	0.46	1.61	0.09	0.39	0.36
Al_2O_3	19.19	19.41	19.54	19.19	19.25	19.51	19.11	19.45	12.97	19.11	16.56	18.45	18.06	19.97
Fe_2O_3	2.63	1.78	3.77	1.78	1.90	3.91	3.16	4.74	3.32	1.98	3.67	4.22	2.27	2.30
FeO	8.52	11.39	9.41	10.68	11.39	23.53	9.00	8.93	26.66	11.93	20.54	10.19	16.53	13.76
MnO	1.03	0.86	1.38	1.22	1.23	0.79	1.84	2.35	1.10	0.83	0.71	1.00	0.59	0.80
ZnO	0.10	0.10	0.14	0.20	0.19	0.12	0.21	0.17	0.72	0.19	0.35	0.22	0.15	0.14
MgO	0.02	0.02	0.05	0.06	0.06	0.05	0.08	0.04	0.10	0.11	0.65	0.08	0.34	0.49
CaO	0.09	0.08	0.08	0.08	0.09	0.09	0.10	0.08	0.14	0.22	0.13	1.61	1.10	0.19
Li_2O	3.81	3.17	2.89	3.12	3.17	0.54	3.23	3.02	0.58	2.97	0.88	2.82	0.71	2.05
Na_2O	0.12	0.16	0.20	0.16	0.13	0.29	0.16	0.22	0.18	0.33	0.19	0.28	0.11	0.14
K_2O	10.32	10.11	9.77	10.26	10.34	9.07	10.51	10.01	8.96	9.74	9.22	9.41	10.08	10.09
Rb_2O	0.42	0.41	0.66	0.50	0.55	0.43	0.55	0.61	0.36	0.69	0.50	0.72	0.54	0.45
Cs_2O	0.002	0.006	0.07	0.07	0.06	0.006	0.02	0.08	0.02	0.08	0.03	0.05	0.02	0.03
P_2O_5	0.08	0.08	0.08	0.08	0.08	0.09	0.09	0.08	0.10	0.06	0.09	0.09	0.11	0.13
H_2O^-	0.30*	0.45	0.30*	---	---	0.30*	0.30*	0.30*	0.19	0.30*	0.30*	0.30*	0.30*	---
H_2O^+	2.83	2.10	3.19	---	---	3.25	3.07	2.98	2.79	3.28	3.45	2.86	2.76	---
F	7.78	7.55	7.24	7.33	7.31	3.47	7.19	6.88	4.12	6.86	4.48	7.99	3.49	5.60
Cl	<0.01	<0.01	---	---	---	0.10	<0.01	<0.01	<0.01	---	<0.01	<0.01	<0.01	---
Subtotal	104.87	101.71	102.06	99.05	98.99	101.59	102.78	102.40	101.11	102.03	101.61	102.89	100.52	99.28
-O = F+Cl	3.28	3.18	3.05	3.09	3.08	1.46	3.03	2.90	1.73	2.89	1.89	3.36	1.47	2.36
Total	101.59	98.53	99.01	95.96	95.91	100.13	99.75	99.50	98.96	99.14	99.72	99.53	99.05	96.92
Ba, ppm	42	46	30	70	59	5	34	38	86	90	403	25	330	210
Sr, ppm	7	12	4	8	12	9	7	8	9	7	19	68	39	26
Tl_2O, ppm	4	8	9	9	10	13	14	12	8	6	10	13	14	10
Ga_2O_3, ppm	121	171	165	107	113	390	107	184	430	123	207	185	375	231
BeO, ppm	86	97	97	114	91	14	105	89	22	144	36	127	33	83
Polytype	1M	1M	1M	1M	1M	$2M_1$	1M	1M	1M	---	3T	---	---	---
Name	Zin.	Zin.	Zin.	Zin.	Zin.	PL	Zin.	Zin.	Sid.	Zin.	PL	Zin.	PL	Zin.

[1] corrected for 1.25 wt. % CaF_2, * 0.30 wt. % H_2O^- used where only total water was determined. *Zin* Zinnwaldite, *Lpd*, Lepidolite, *Ms* Muscovite, *Phl* Phogopite # FeO/Fe_2O_3 set equal to 6.0 because of lack of determination of ferrous iron. --- not determined. *PL* 'Protolithionite' (siderophyllite), *Sid* Siderophyllite

Table 3. *Empirical formulas for Li-Fe and other micas from miarolitic pegmatities of the Pikes peak batholith*

	1a	**1b**	**2**	**3**	**4**	**5**	**8**	**9**	**86-25**	**86-26**	**86-27**	**21**	**22**	**23**	**24-1**
Tetrahedral site															
Si	6.50	6.71	5.93	5.91	6.03	5.81	6.61	6.28	6.41	6.25	6.57	6.90	6.62	6.55	6.30
Al(IV)	1.50	1.29	2.07	2.09	1.97	2.19	1.39	1.72	1.59	1.75	1.43	1.10	1.38	1.44	1.70
octahedral site															
Al(VI)	1.94	1.96	1.39	1.34	3.10	0.52	2.04	2.04	1.91	1.92	1.94	1.90	2.10	1.65	1.75
Ti	0.04	0.02	0.02	0.02	0.02	0.31	0.02	0.02	0.00	0.01	0.01	0.01	0.04	0.02	0.01
Fe^{3+}	0.13	0.12	0.30	0.27	0.07	0.50	0.14	0.22	0.14	0.07	0.18	0.06	0.04	0.22	0.09
Fe^{2+}	1.47	1.07	2.39	2.45	0.40	1.80	1.15	1.52	1.59	1.41	1.39	0.97	1.71	1.48	1.49
Mg	0.08	0.04	0.11	0.16	0.03	2.27	0.10	0.08	0.02	0.00	0.03	0.02	0.04	0.02	0.00
Mn	0.12	0.09	0.16	0.12	0.09	0.11	0.10	0.11	0.15	0.51	0.20	0.11	0.07	0.02	0.25
Zn	0.02	0.02	--	--	--	--	--	--	0.01	0.02	0.02	0.01	0.02	0.01	0.02
Li	2.01	2.41	0.61	0.65	0.59	0.04	1.43	1.46	1.88	1.81	1.80	2.93	1.62	2.26	1.59
Σ	5.81	5.73	4.97	5.01	4.30	5.55	4.98	5.45	5.70	5.75	5.57	6.01	5.64	5.68	5.20
Interlayer site															
Ca	0.01	0.01	0.02	0.01	0.01	0.02	0.01	0.01	0.01	0.05	0.05	0.02	0.01	0.02	0.02
Na	0.06	0.09	0.13	0.16	0.15	0.17	0.10	0.07	0.05	0.06	0.05	0.05	0.04	0.03	0.09
K	1.85	1.88	1.86	1.84	1.77	1.86	1.86	1.86	1.89	1.80	1.78	1.93	1.96	1.93	1.79
Rb	0.06	0.05	0.06	0.06	0.05	0.01	0.03	0.05	0.03	0.08	0.06	0.04	0.05	0.05	0.09
Cs	0.00	0.00	0.00	0.00	0.01	0.00	0.01	0.00	0.00	0.00	0.00	0.00	0.00	0.00	0.00
Σ	1.97	2.03	2.07	2.07	1.99	2.06	2.01	1.99	1.98	1.99	1.94	2.04	2.06	2.03	1.99
Anion site															
OH	0.82	1.03	1.88	2.00	2.93	2.90	0.71	1.71	0.54	0.59	0.54	2.10	1.80	--	1.64
F	2.89	2.97	2.12	2.00	1.07	0.70	3.29	2.24	3.46	3.41	3.46	1.88	1.62	--	1.66
O	0.29	---	---	---	---	0.40	---	0.05	---	---	---	0.02	0.58	--	0.70
excess OH	---	0.06	0.93	0.96	0.80	---	0.65	---	0.60	0.15	0.09	---	---	--	---
Σ	4.0	4.0	4.0	4.0	4.0	4.0	4.0	4.0	4.0	4.0	4.0	4.0	4.0	--	4.0

Table 3. (*Continued*)

	24-2a	24-2b	25a	25b	25c	26	27	41	42	43	45	46	47	48
Tetrahedral site														
Si	6.71	6.56	6.34	6.57	6.47	5.62	6.43	6.33	6.07	6.43	5.94	6.31	6.53	6.33
P	0.01	0.01	0.01	0.01	0.01	0.01	0.01	0.01	0.01	0.01	0.01	0.01	0.01	0.02
Al(IV)	1.28	1.43	1.65	1.42	1.52	2.37	1.56	1.66	1.92	1.56	2.05	1.68	1.46	1.65
Octahedral site														
Al(VI)	1.90	1.98	1.73	1.94	1.86	1.24	1.73	1.76	0.58	1.82	0.98	1.55	1.78	1.83
Ti	0.00	0.00	0.02	0.01	0.02	0.05	0.02	0.01	0.15	0.05	0.19	0.01	0.04	0.04
Fe^{3+}	0.28	0.20	0.42	0.20	0.21	0.46	0.35	0.53	0.41	0.22	0.43	0.47	0.26	0.26
Fe^{2+}	1.00	1.42	1.16	1.33	1.42	3.09	1.10	1.11	3.64	1.50	2.67	1.26	2.10	1.70
Mg	0.00	0.00	0.01	0.01	0.01	0.01	0.02	0.01	0.02	0.03	0.15	0.02	0.08	0.11
Mn	0.12	0.11	0.17	0.15	0.16	0.10	0.23	0.30	0.15	0.11	0.09	0.13	0.08	0.10
Zn	0.01	0.01	0.01	0.02	0.02	0.01	0.02	0.02	0.09	0.02	0.04	0.02	0.01	0.02
Li	2.16	1.90	1.71	1.86	1.90	0.34	1.90	1.81	0.38	1.79	0.55	1.68	0.43	1.22
Σ	5.47	5.62	5.23	5.52	5.39	5.30	5.37	5.55	5.42	5.54	5.10	5.14	4.78	5.28
Interlayer site														
Ca	0.01	0.01	0.01	0.01	0.01	0.02	0.02	0.01	0.02	0.04	0.02	0.26	0.18	0.03
Na	0.03	0.05	0.06	0.05	0.04	0.09	0.05	0.06	0.06	0.10	0.06	0.08	0.03	0.04
K	1.85	1.92	1.83	1.94	1.97	1.82	1.96	1.91	1.87	1.86	1.83	1.78	1.95	1.91
Rb	0.04	0.04	0.06	0.05	0.05	0.04	0.05	0.06	0.04	0.07	0.05	0.07	0.05	0.04
Cs	0.00	0.00	0.00	0.00	0.00	0.00	0.00	0.00	0.00	0.00	0.00	0.00	0.00	0.00
Σ	1.93	2.02	1.96	2.04	2.06	1.97	2.06	2.04	1.99	2.03	1.96	2.19	2.21	2.02
Anion site														
OH	2.27	1.96	2.32	---	---	3.14	2.34	2.38	2.94	0.74	2.90	2.13	2.94	---
F	1.73	1.78	1.68	---	---	0.86	1.66	1.62	1.06	3.26	1.10	1.87	0.84	---
O	--	0.26	--	---	---	--	--	--	--	--	--	--	0.22	---
excess OH	0.36	--	0.72	---	---	0.32	0.54	0.56	0.10	2.54	0.72	0.64	--	---
Σ	4.0	4.0	4.0	--	--	4.0	4.0	4.0	4.0	4.0	4.0	4.0	4.0	--

Formulas calculated according to the method of *Foster* (1960a)

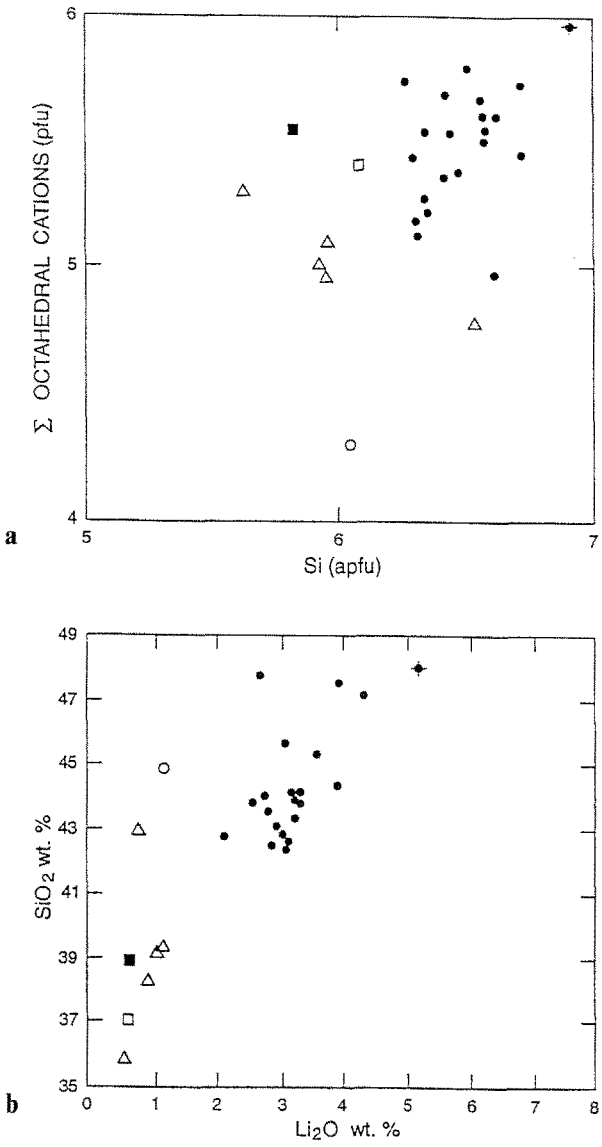

Fig. 4. **a** Si vs. sum of octahedral cations (a.p.f.u.) for micas from PPB pegmatites. Symbols: solid circles – zinnwaldite, open triangles – lithian biotite, solid circle with spikes – ferroan lepidolite, solid square – phlogopite, open square – siderophyllite, and open circle – muscovite. Diagram modified from Černý and *Burt* (1984). **b** SiO_2 vs. Li_2O (wt. %) plot for micas from PPB pegmatites. Symbols: open triangles – lithian biotite, open square – siderophyllite, solid square – phlogopite, open circle – muscovite, solid circles – zinnwaldite, and solid circle with spikes – ferroan lepidolite

The SiO_2 abundance increases from siderophyllite through phlogopite and lithian biotite to muscovite, zinnwaldite and ferroan lepidolite, roughly parallel with the increase in Li_2O (Fig. 4b). Al_2O_3 contents vary in a similar manner; they reach a maximum in muscovite and decrease in lepidolite below the level typical of zinnwaldite samples. In terms of atoms *p.f.u.* (per formula unit), Si increases from muscovite through average lithian biotite and zinnwaldite to lepidolite, parallel to the increase in Li (Fig. 4a). This is also shown on Fig. 5, a vector diagram from *Černý* and *Burt* (1984). The well-known positive correlation between Li and F is somewhat approximate but continuous throughout the sequence of different mica species (Fig. 6a). In contrast, the correlation of H_2O^+ and F is very poor, particularly in zinnwaldite (Fig. 6b). This confirms the inference that H_2O may also be present in forms other than (OH), as mentioned in Instrumentation and Methods.

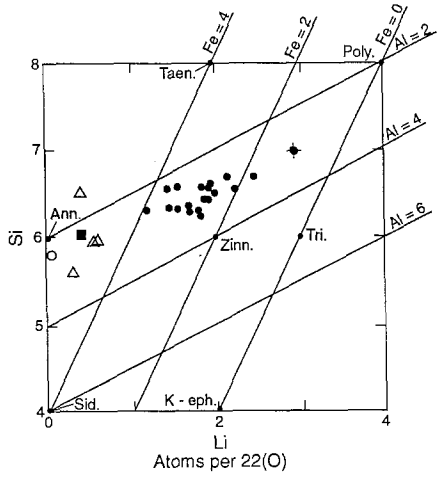

Fig. 5. Vector diagram (atomic) for analyzed micas from PPB pegmatites. Note that the Al contents refer to the sum of octahedral and tetrahedral Al. *Sid* siderophyllite, *Ann* annite, *K-eph* K-ephesite, *Tri* trilithionite, *Poly* polylithionite, *Taen* taeniolite, *Zinn* zinnwaldite. Diagram from *Černý* and *Burt* (1984). Symbols: solid circles – zinnwaldite, solid circle with spikes – ferroan lepidolite, open square – siderophyllite, open triangles – lithian biotite, and solid circle – phlogopite

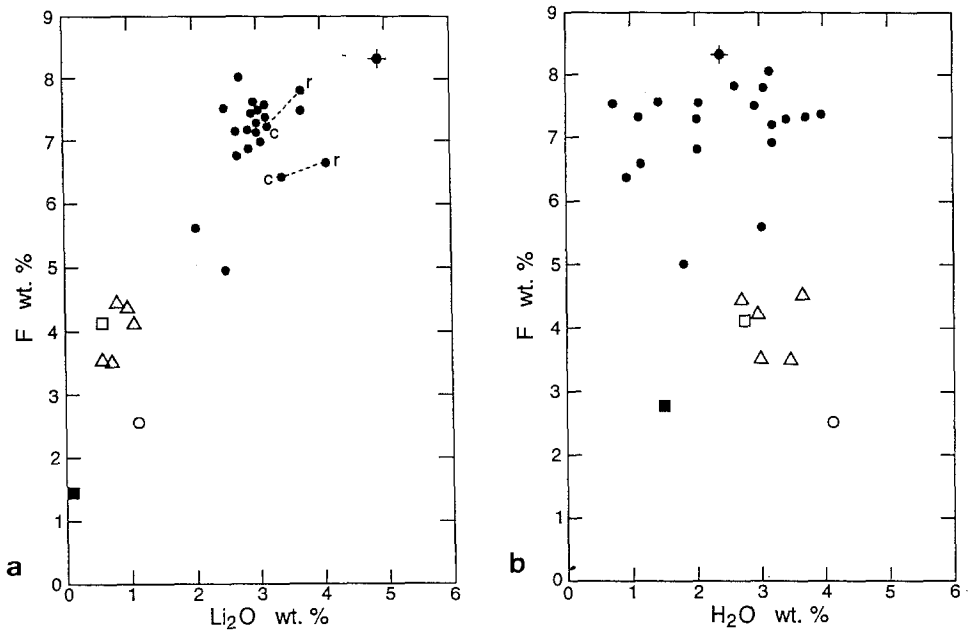

Fig. 6. **a** Li_2O vs. F (wt. %) plot for micas from PPB pegmatites. Symbols: solid square – phlogopite, open circle – muscovite, open square-siderophyllite, open triangles – lithian biotite, solid circles – zinnwaldite, and solid circle with spikes – ferroan lepidolite. *r* rim, *c* core. **b** F vs. H_2O+(wt. %) plot for micas from PPB pegmatites. Symbols: solid square – phlogopite, open square – siderophyllite, open circle – muscovite, open triangles – lithian biotites, solid circles – zinnwaldites, and solid circle with spikes – ferroan lepidolite

A plot (Fig. 7) of FeO (total Fe as FeO) vs. SiO_2 also shows a linear trend for the mica sequence from siderophyllite to ferroan lepidolite. The zinnwaldites show a fairly coherent grouping.

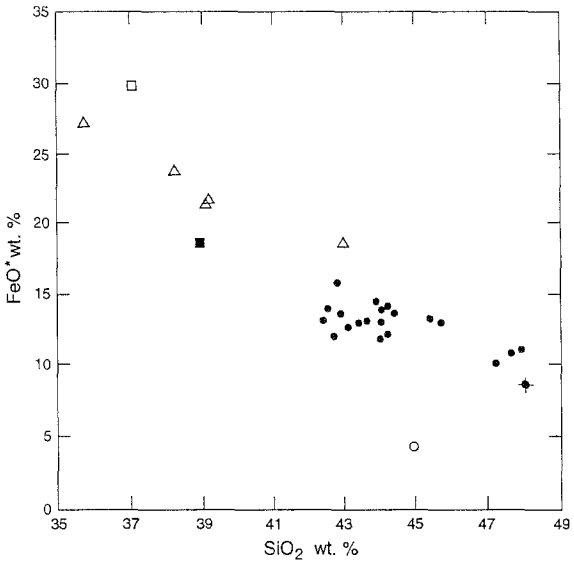

Fig. 7. Total iron as FeO vs. SiO_2 (wt. %) plot for micas from PPB pegmatites. Symbols: solid circles – zinnwaldite, solid circle with spikes – ferroan lepidolite, open triangles – lithian biotite, solid square – phlogopite, open square – siderophyllite, and open circle – muscovite

Table 4. *INAA results for selected pegmatitic micas from the Pikes Peak batholith*

Element	Sample no.								
			core	intermed.	rim		rim	intermed.	core
	48	86-25	1a	1 intermed	1b	26	25a	25b	25c
Cs	160	113	227	525	322	48	408	612	658
Sc	43	37	55	46	32	104	22	31	4556
Rb	4428	2433	5951	4196	5026	3453	—	4470	—
Zn	1586	990	1718	1380	11340	834	—	1733	—
Ta	46	126	133	69	16	122	—	64	—
	25 core	25 rim	24-1						
Cs	293	171	183						
Sc	45	34	35						
Rb	6086	4489	6747						
Zn	1163	1118	1042						
Ta	68	92	119						

Note: Sample numbers are the same as those given in Table 1 and 2, along with some additional zones. All values given in parts per million (ppm)

INAA analysis

Partial analysis for twelve samples show a very good agreement between the INAA values and the contents determined by atomic absorption, flame photometry, or ICP-AES for those elements in common (Cs, Rb, Zn) and provides greater confidence about the accuracy of the chemical analyses. Table 4 contains INAA values determined for selected elements. The Zn content of the outermost zone of one color-zoned zinnwaldite crystal from an open pocket cavity was 1.13% wt. %. Usually Zn is about 0.1 wt. %.

Mössbauer studies

Zinnwaldite has been studied by Mössbauer and other optical spectral techniques (see *Rossman*, 1984). *Levillain* et al. (1981) presented Mössbauer data for synthetic and natural micas along the siderophyllite-polylithionite join. The amount of Fe^{3+} determined by Mössbauer spectroscopy for the various mica samples (one siderophyllite, one lithian biotite, and seven zinnwaldites) is both higher (siderophyllite and zinnwaldite) and lower (Li-biotite) than that determined by wet chemistry. *Rossman* (1984) has discussed oxidation of iron during sample dissolution for wet chemical analysis. Core and rim portions of two samples of color- and compositionally zoned zinnwaldite (one from Wigwam Creek – samples 1a and 1b, and one from Harris Park) were analyzed by Mössbauer spectroscopy. Neither showed much difference in the amount of Fe^{3+} as a function of position relative to color-zonation. The colorless core portion of the zinnwaldite from Harris Park contains about 4% Fe^{3+} (of the total Fe) and the medium brown rim contains about 6.5% Fe^{3+}. Similarly, the red-brown core portion of sample 1a contains about 20% Fe^{3+} and the pale yellow-brown rim portion (1b) contains about 16.5% Fe^{3+}. In both cases, the amount of Fe^{3+} (relative to total Fe) correlates with the intensity of color in the mica. The changes in color zoning also correlate well with TiO_2 content (Table 2) as determined by electron-microprobe traverses.

Polytypism

Polytypes were determined for 22 of the 29 mica samples. All zinnwaldites are 1M polytype, the ferroan lepidolite is 1M, the one sample of muscovite is $2M_1$, the single phlogopite sample is probably 1M, and the siderophyllite (no. 42) is 1M. Lithian biotite shows the 3T polytype (three samples) and the $2M_1$ polytype (one sample).

Physical properties

Megascopic colors of the mica samples range from black to pale yellowish tan. In thin flakes, colors range from colorless (muscovite and zinnwaldites) to shades of green, blue-green and gray-green (lithian biotite and siderophyllite) to various shades of tan, red-brown, and orange-brown (zinnwaldite and ferroan lepidolite). All five samples of lithian biotite are various shades of green in thin (<0.05 mm) slices, and the color distribution was uniform. The green color may arise from Fe^{2+}/Fe^{3+} IVCT (intervalence charge transfer) (*Rossman*, 1984). The zinnwaldites, on the other hand, are generally complexly color-zoned, showing a wide variation in color. Figures 3a and 3b show compositional growth zoning in two different crystals of zinnwaldite. The varying shades of yellow, reddish brown, and orange correlate well with TiO_2 content. Darker colored zones contain from 0.2 to 0.6 wt. % TiO_2 whereas light colored zones or colorless zones contain 0.25 wt. % TiO_2 or less. Microprobe traverses show that the TiO_2 content changes abruptly at color boundaries. The color-zoning may be due to Fe^{2+}-Ti^{4+} IVCT processes (*Rossman*, 1984). Almost no Fe^{2+}/Fe^{3+} IVCT was identified by *Rossman* (1984) in the zinnwaldite from Wigwam Creek (1a, 1b).

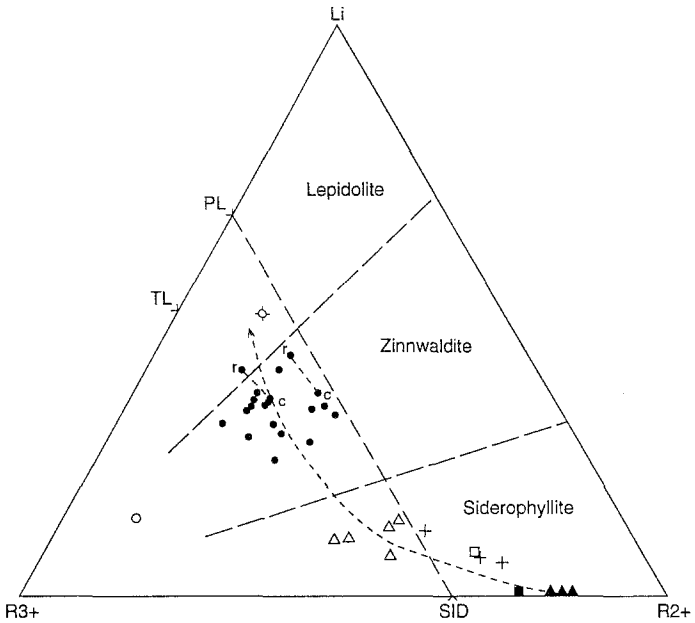

Fig. 8. Li-R^{3+} (Al, Ti, Fe)-R^{2+}(Fe, Mg, Mn, Zn) octahedral site population plot for micas from PPB pegmatites and from host-granite units. Boundaries demarcating fields of lepidolite, zinnwaldite, and siderophyllite are from *Stone* et al. (1988). Symbols: open circle – muscovite, open triangles – lithian biotite, plus signs – annites from *Hawley* and *Wobus* (1977), solid square – phlogopite, solid triangles – annites from *Barker* et al. (1975), open square – siderophyllite, solid circles – zinnwaldite, and solid circle with spikes – ferroan lepidolite. *r* rim portion and *c* core portion of zoned zinnwaldite crystals. Evolution trend line is indicated. *PL* polylithionite, *TL* trilithionite, *SID* siderophyllite

Geochemical evolution of the micas

Figure 8 shows compositions of the analyzed micas, complemented by annite specimens analyzed by *Barker* et al. (1975) and by *Hawley* and *Wobus* (1977), on the "Foster diagram" of R^{3+}-R^{2+}-Li. The paragenetic succession from the plutonic annite through siderophyllite (of *Rieder*, 1970) to lithian biotite (siderophyllite of *Stone* et al., 1988) to zinnwaldite and ferroan lepidolite (cryophyllite of *Foster* and *Evans*, 1962) follows an arcuate trend of decreasing R^{2+} (mainly Fe), increasing Li and, as shown in Figs. 4b, 5, 6a, and 6b, increasing Si and F.

Isolated occurrences of early (ferrous) phlogopite and late muscovite are apparently due to specific local aberrations from the main trend, the reasons for which are indeterminate without an intimate knowledge of the paragenetic position of these micas and information on the chemistry of associated (and preceding) phases.

As shown in Fig. 9a, Mg abundances decrease in progressively more evolved micas; Ti abundances show a similar trend. In contrast, Mn increases but only very slightly and erratically (Fig. 9b).

Figures 10a and 10b show that both K/Rb and Rb/Cs are variable over rather restricted ranges, 33–9 and (with two exceptions) 33–4, respectively. Neither of these ratios is well correlated with Li abundance variations, which may, to a large extent, reflect the sampling of diverse miarolitic cavities and pegmatites within several

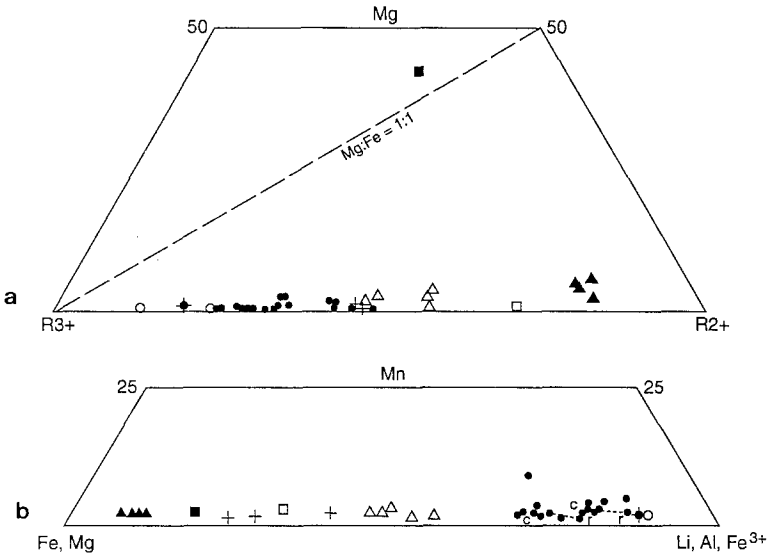

Fig. 9. **a** Mg-R^{3+} (Al, Ti, Fe)-R^{2+} (Fe, Mg, Mn, Zn) octahedral site population plot for the same sample shown in Fig. 8. Symbols are the same as for Fig. 8. **b** (Li-Al-Fe^{3+})-Mn-R^{2+}(Fe, Mg) octahedral site population plot for the same samples shown in Figs. 8 and 9a. Symbols are the same as for Figs. 8 and 9a

igneous centers. Unfortunately, paragenetic sequences of micas from single sections across a pegmatite and its cavity could not be collected and examined. Mica suites of this kind could, and virtually should, show progressive fractionation trends indicative of closed or nearly closed system crystallization.

In view of the above scatter of Rb and Cs data, it is all the more surprising to find a well-defined trend in the Al/Ga ratios (Fig. 11), evolving regularly with the increase in Li, more or less smoothly throughout the sequence of mica species. The most remarkable feature of that trend is the extremely low Al/Ga ratio (about 250) in early micas, gradually increasing to very high values in the late, cavity-lining micas (about 2000 to 2200).

Other trace elements are present in variable quantities. Tl is consistently very low (3–15 ppm) and Sc abundances are moderate within a narrow range (22–104 ppm, except for one high value; Table 3). In contrast, Ba (5–400 ppm), Be (3–198 ppm), Sn (4–68 ppm) and Ta (16–133 ppm) show much broader ranges but no distinct trends relative to major or minor elements. The average content of Sn of three zinnwaldites is 150 ppm. The content of Zn is considerably elevated, ranging from 834 to 11340 ppm (Tables 3 and 4). Elevated levels of lithophile elements were also found in early annite by *Hawley* and *Wobus* (1977). Most zinnwaldite crystals show a decrease in total iron and MgO from core to rim (Figs. 8 and 9b). In contrast, Li_2O, SiO_2 and F increase (Fig. 8) whereas MnO, Rb_2O, Cs_2O, and Na_2O remain essentially constant. Total $FeO + Fe_2O_3$ ranges from 19 to 30 wt. % for siderophyllite and lithian biotite, and from 10.1 to 16.1 wt. % for zinnwaldite. The one sample of ferroan lepidolite has a total $FeO + Fe_2O_3$ content of 8.7 wt. %. TiO_2 also follows a decreasing trend with continued crystallization. The ratio FeO/Fe_2O_3 is variable, but a narrow range of 5 to 8 is observed for early siderophyllite and lithian biotite.

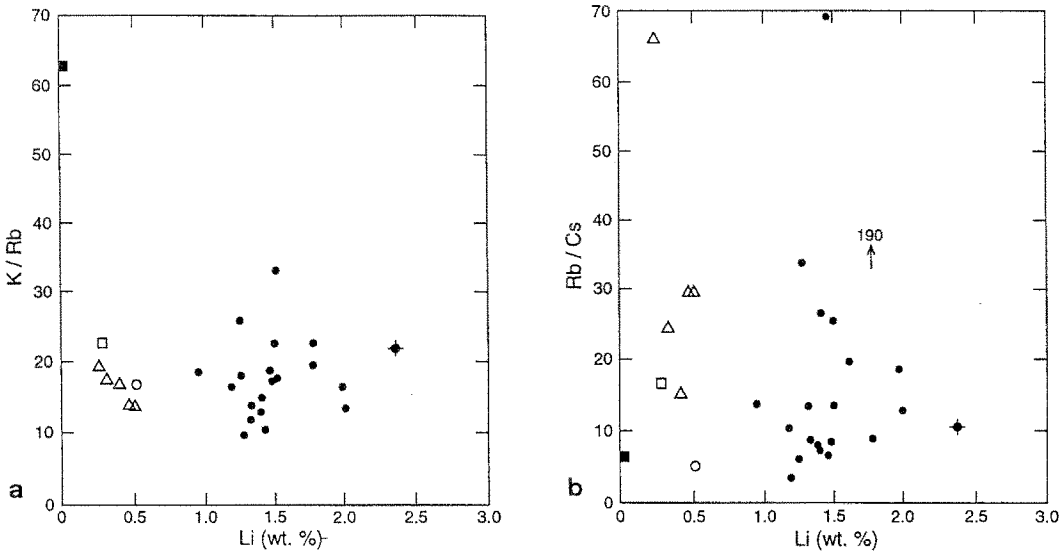

Fig. 10. **a** K/Rb vs. Li (atomic) plot for micas from PPB pegmatites. Symbols as in Figs. 4b and 6b % **b** Rb/Cs vs. Li. (atomic) plot for micas from PPB pegmatites. Symbols as in Figs. 4b, 6b, 10a

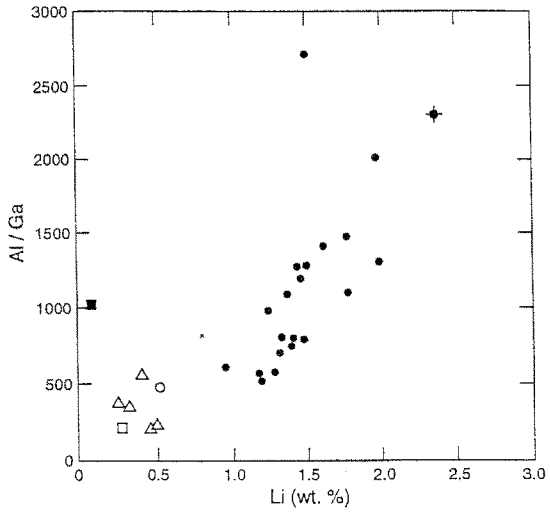

Fig. 11. Al/Ga vs. Li (atomic) plot for micas from PPB pegmatites. Symbols as in Figs. 4b, 6b, 10a, and 10b

Later cavity-grown zinnwaldite shows a much broader variation from 2 to 40 that in part correlates with Ti abundance oscillations. Variations in $f(O_2)$, caused by episodic leaks of O-rich vapor phase from the vugs, may be the principal cause.

MnO contents range between 0.53 and 2.35 wt. % for 26 lithian biotite and zinnwaldite specimens; one additional zinnwaldite sample contains about 4 wt. % MnO, indicating the presence of a significant masutomilite component. Masutomilite, zoned zinnwaldite-masutomillite, and manganoan zinnwaldite from other occurrences have been discussed by *Harada* et al. (1976, 1990), *Lowell* and *Tobey* (1979), *Němec* (1983a, b) and *Menzies* and *Boggs* (1993).

The succession of the compositions for micas from pegmatites of the PPB corresponds well to that determined by *Ponomareva* et al. (1993) for micas from

"chamber" pegmatites, which reflects decreasing temperature, alkalinity and a(Fe), and increasing a(Li,F).

As emphasized by *Rieder* (1971), Li and F increase in about a 1:1 atomic ratio along the siderophyllite-polylithionite join. Experimental studies show that annite is stable only in F-poor environments, e. g. PPB granitic units. Thus, the pegmatitic micas are siderophyllite through ferroan lepidolite because of the abundance of F in the pegmatite systems.

Late alteration

For reasons still not clear to us, most of the mica deposited in the border or contact zone, and graphic Fs-Qtz zone, is completely altered to vermiculite. Much of the Li-Fe mica present within quartz-filled or open pocket cavities is also altered to vermiculite and/or chlorite. The presence or absence of altered material in these cavities may be due to a considerable degree of reaction between micas and late-stage hydrothermal fluids circulating in the pegmatites. The contents of SiO_2, K_2O, and Al_2O_3 decrease and those of total iron and ferric iron, CaO, and H_2O^+ increase during the alteration of the micas to vermiculite.

A chemical analysis of a vermiculite pseudomorph after a pseudohexagonal, barrel-shaped crystal of zinnwaldite from the edge of a miarolitic cavity in a pegmatite near Hackett Gulch gave (in wt. %) SiO_2 32.23, TiO_2 1.78, Al_2O_3 15.00, Fe_2O_3 13.65, FeO 17.94, MnO 0.73, ZnO 0.30, MgO 1.84; CaO 4.80, Li_2O 0.13, Na_2O 0.03, K_2O 1.51; Rb_2O 0.04, Cs_2O 0.003, P_2O_5 0.10, H_2O^- 0.22, H_2O^+ 7.86, F 3.32, Cl < 0.01, subtotal 101.48, O = F + Cl 1.40, total 100.08. Trace element abundances are: Ba 272 ppm, Sr 45 ppm, Tl_2O 5 ppm, Ga_2O_3 1440 ppm, BeO 39 ppm. It is not possible to calculate an empirical formula for the vermiculite because the sample was not completely converted to vermiculite and some fine-grained fluorite is also present.

Evidence for late-stage hydrothermal activity within some pegmatite dikes and bodies is indicated by the presence of infilling chlorite and/or smectite. Pocket-filling clays, zeolites, chlorite, etc. in peraluminous LCT(Li-Cs-Ta) granitic pegmatites were discussed in detail by *Foord* et al. (1986) and *Taylor* and *Foord* (1993). However, such studies of pocket-filling clays in anorogenic granitic pegmatites are still lacking. The chemical composition of fine-grained, clay-like, olive-green aluminian clinochlore II-b, filling a miarolitic cavity in a pegmatite on the Wigwam Creek no. 2 claim (same location, but different miarolitic cavity, for zinnwaldite samples 1a and 1b), is as follows (wt. %): SiO_2 30.7 wt. %, Al_2O_3 20.1, FeO 13.24, Fe_2O_3 8.28, MgO 12.5, CaO 0.77, K_2O 0.62, MnO 0.19, $H_2O_{(tot)}$ 12.9, F 0.49, total 99.79, O for F 0.21, total 99.58. The analysis was done by X-ray fluorescence methods and the ferrous-ferric iron ratio determined from a Mössbauer spectrum. An empirical formula calculated on the basis of 18 oxygen atoms is:

$$(Mg_{1.85}Fe^{2+}_{1.10}\square_{0.85}Fe^{3+}_{0.62}Al_{0.40}Ca_{0.08}K_{0.08}Mn_{0.02})_{\Sigma 5.00}$$
$$Al(Si_{3.05}Al_{0.95})O_{10}(OH_{8.55}F_{0.15})_{\Sigma 8.70}.$$

An 0.85 cation vacancy is indicated for the octahedral site because of the presence of trivalent Al and Fe, and some of the water is most likely H_2O^- because of the 0.7 excess negative charge present.

Early siderophyllite (#42) contained approximately 23% ferric iron as determined by Mössbauer spectroscopy. In the case of one sample of lithian biotite and five out of seven of the zinnwaldites examined in this study, the amount of ferric iron was shown to be less than about 10% of the total iron, indicating strongly reducing conditions even during the final stages of pocket formation. One zinnwaldite crystal (1a, 1b) showed 16.5–20% ferric iron. Alteration of these micas into vermiculite with Fe^{3+}/Fe^{2+} about 1, deposition of Fe^{3+}-rich minerals such as chlorite, hematite, goethite (pseudomorphous after siderite, manganoan siderite or rhodochrosite) indicates action of later oxygenated hydrothermal solutions postdating pocket formation proper. Some additional alteration may be due to supergene weathering processes.

Comparison with other mica suites in granitic pegmatites

The only other mica sequence from NYF-related miarolitic pegmatites which was investigated to date is that from the "chamber" pegmatites of the Korosten pluton, Volynia, Ukraine (*Lazarenko* et al., 1973). Data on minor elements are not reliable but the bulk compositions of the Korosten micas closely follow the trend identified in the present study (Fig. 12a). Some other micas from pegmatites reportedly associated with A-type granites also fall within the broad range of this trend (Fig. 12b). The general earmarks of these micas are their iron-rich chemistry (persisting to

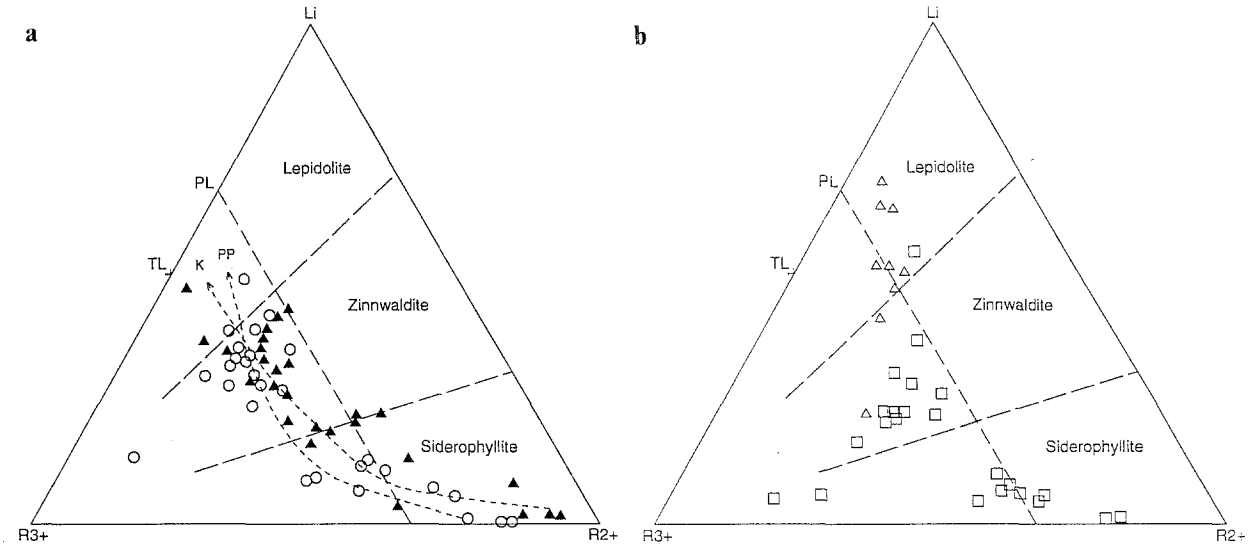

Fig. 12. **a** Li-R^{3+} (Al, Ti, Fe)-R^{2+} (Fe, Mg, Mn, Zn) octahedral site population plot for micas for PPB pegmatites, host-granite units, and micas from pegmatites of the Korosten pluton, Volynia, Ukraine. Symbols: open circles – PPB, solid triangles – Korosten pluton, Volynia, Ukraine (From *Černý* and *Burt*, 1984). Evolution trend lines for PPB micas (PP) and Korosten pluton micas (K) are indicated. Field boundaries are from *Stone* et al. (1988). **b** Li-R^{3+} (Al, Ti, Fe)-R^{2+}(Fe, Mg, Mn, Zn) octahedral site population plot for micas from anorogenic granites in Saudi Arabia (*du Bray*, 1994) and other occurrences. Symbols: open triangles – other world occurrences (from *Černý* and *Burt*, 1984), open squares – Saudian Arabian shield (*du Bray*, 1994). Field boundaries are from *Stone* et al. (1988)

a degree to the most fractionated members), relatively low Rb, Cs, and Tl contents but enhanced Zn and Sc.

In contrast, the "internal" micas of the peraluminous pegmatites of the LCT family are usually very poor in Fe, Mg, Zn, and Sc (except for biotite from the outermost border zones) and considerably enriched in Rb, Cs, and Tl (cf. *Hawthorne* and *Černý*, 1982; *Černý* and *Burt*, 1984; *Černý* et al., 1993). The only trioctahedral micas from the LCT pegmatites that may be remotely similar to those examined in the present study are those from exocontact aureoles in mafic host rocks. However, their bulk compositions fall largely outside the trends of Fig. 12b, and they tend to be aligned across these trends (*Hawthorne* and Černý, 1982; *Černý* and *Burt*, 1984).

Conclusions

This study provides chemical data for micas from the miarolitic pegmatites generated by the PPB. Crystallization of homogeneous annite throughout the fine to coarse-grained plutonic units of the batholith was followed by crystallization of siderophyllite – lithian biotite – zinnwaldite – ferroan lepidolite with continued fractionation of the pegmatites. All of the pegmatitic micas are primary based on textural and compositional data, as formulated by *Henderson* et al. (1989). These micas are the products of extreme fractionation of a subaluminous anorogenic granitic melt. Strong enrichment of Li, Rb, and F is indicated; elevated Zn contents are characteristic of A-type, NYF-family granites and pegmatites. The sharp color and compositional zoning of the zinnwaldite and ferroan lepidolite crystals in miarolitic cavities reflects rapid fluctuations in the composition of the parent fluid phase, mainly in $f(O_2)$ episodically reduced via loss of vapor phase from the vugs or cavities. Alteration to vermiculite and filling of cavities with Fe^{3+}-rich minerals resulted probably from the action of late, unrelated fluids.

Acknowledgments

The authors thank the following people for providing samples for study: *D. E. Kile* (USGS), *B. R. Kinney, T. C. Michalski* (USGS), *R. G. Bennett, W. H. Hayward* and *D. S. Collins* (USGS). All of the foregoing are dedicated and observant field collectors. We thank Dr. *W. B. Simmons*, Univ. of New Orleans-Lakefront for providing INA analyses of mica samples. Some of the laboratory work was supported by NSERC of Canada operating grant to *P. Č.* We thank *V. J. Kubat* (Ecole Polytechnique) and *W. Blonsky* (University of Manitoba) for chemical analyses. Reviews were provided by *T. C. Michalski, E. A. du Bray, W. B. Simmons* and *A. U. Falster*. Their comments and suggestions are much appreciated.

References

Bailey SW (1984) Appendix 2-X-ray identification of mica polytypes: In: *Bailey S W* (ed) Reviews in mineralogy, vol 13. Micas. Mineral Soc of America, 10 pp

Barker F, Wones DR, Sharp WN, Desborough GA (1975) The Pikes Peak Batholith, Colorado Front Range, and a model for the origin of the gabbro-anorthosite-syenite-potassic granite suite. Precam Res 2: 97–160

Blasi A, Brajkovic A, De Pol Blasi C, Foord EE, Martin RF, Zanazzi PF (1984) Structure refinement and genetic aspects of a microcline overgrowth on amazonite from Pikes Peak batholith, Colorado, U.S.A. Bull de Mineral 107: 411–422

Černý *P* (1991a) Rare-element granitic pegmatites, part I. Anatomy and internal evolution of pegmatite deposits. Geosci Canada 18: 49–67

Černý P (1991b) Rare-element granitic pegmatites, part II. Regional to global environments and petrogenesis. Geosci Canada 18: 68–81

Černý P (1991c) Fertile granites of Precambrian rare-element pegmatite fields: is geochemistry controlled by tectonic setting or source lithologies? Precam Res 51: 429–468

Černý P (1992) Geochemical and petrogenetic features of mineralization in rare-element granitic pegmatites in the light of current research. Appl Geochem 7: 393–416

Černý P, Burt DM (1984) Paragenesis, crystallochemical characteristics, and geochemical evolution of micas in granite pegmatites: In: *Bailey SW*(ed) Reviews in mineralogy, vol 13. Micas. Mineral Soc of America, pp 257–297

Černý P, London D (1983) Crystal chemistry and stability of petalite. Tschermak's Mineral Petrogr Mitt 31: 81–96

Černý P, Stanek J, Novák M, Baadsgaard H, Rieder M, Ottolini L, Chapman R (1995) Geochemical and structural evolution of micas in the Rožná and Dobrá Voda pegmatites, Czech Republic. Mineral Petrol 55 (this volume)

Clark FW (1887) 4. Iron-mica from near Pike's Peak. Am J Sci (third series) 34 200: 136–137

Colby JW (1968) Quantitative microprobe analysis of thin insulating films. Adv X-ray Analyses 11: 287–305

Deer WA, Howie RA, Zussman J (1966) An introduction to the rock-forming minerals. Longman and Sons, New York, 528 pp

DePaolo DJ (1981) Neodymium isotopes in the Colorado Front Range and crust-mantle evolution in the Proterozoic. Nature 291: 193–196

Desborough GA, Luddington SD, Sharp WN (1980) Redskin Granite: a rare-metal-rich Precambrian pluton, Colorado, USA. Mineral Mag 43: 959–966

du Bray EA (1994) Compositions of micas in peraluminous granitoids of the eastern Arabian shield-implications for petrogenesis and tectonic setting of highly evolved, rare-metal enriched granites. Contrib Mineral Petrol 116: 381–397

Dyar MD, Burns RG (1986) Mössbauer spectral study of ferruginous one-layer trioctahedral micas. Am Mineral 71: 955–965

Foord EE, Martin RF (1979) Amazonite from the Pikes Peak Batholith. Mineral Rec 10: 373–384

Foord EE, Starkey HC, Taggart JE (1986) Mineralogy and paragenesis of 'Pocket clays' and associated minerals in complex granitic pegmatites, San Diego County, California. Am Mineral 71: 428–439

Foster MD (1960a) Interpretation of the composition of trioctahedral micas. US Geol Survey Prof Paper 354-B, 11–49

Foster MD (1960b) Interpretation of the composition of lithium micas. US Geol Survey Prof Paper 354-E, 115–147

Foster MD, Evans HT(1962) New study of cryophyllite. Am Mineral 47: 344–352

Fratta M (1974) AAS determination of ppb amounts of thallium in silicate rocks. Can Spectroscopy 19: 33–37

Gordiyenko VV, Semenova TF, Simakova YuS (1991) Composition and polytypism of aluminous micas in granitic pegmatites. Mineralogicheski Zhur 12: 67–84 (in Russian)

Gross EB, Heinrich EW(1965) Petrology and mineralogy of the Mount Rosa area, El Paso and Teller Counties, Colorado. I. The granites. Am Mineral 50: 1273–1295

Harada K, Honda M, Nagashima K, Kanisawa S (1976) Masutomilite, manganese analogue of zinnwaldite, with special reference to masutomilite-lepidolite-zinnwaldite series. Mineral J (Japan) 8: 95–109

Harada K, Kanisawa S, Tomita K (1990) Five manganoan zinnwaldites from Japanese pegmatites. Mineral J (Japan) 15: 73–80

Hawley CC, Wobus RA (1977) General geology and petrology of the Precambrian crystalline rocks, Park and Jefferson Counties, Colorado. US Geol Survey Prof Paper 608-B, 77 pp

Hawthorne FC, Černý P (1982) The mica group. In: *Černý P* (ed) Short course in granitic pegmatites in science and industry. Mineral Assoc Canada 8: 63–98

Henderson CMB, Martin JS, Mason RA (1989) Compositional relations in Li-micas from S.W. England and France: an ion-and electron-microprobe study. Mineral Mag 53: 427–449

Jolliff BL, Papike JJ, Shearer CK (1987) Fractionation trends in mica and tourmaline as indicators of pegmatite internal evolution: Bob Ingersoll pegmatite, Black Hills, South Dakota. Geochim Cosmochim Acta 51: 519–534

Lazarenko EK, Pavlishin VI, Latysh VT, Sorokin YuG (1973) Mineralogy and genesis of the chamber pegmatites of Volynia. Lvov State Univ Publishing House, Lvov, 359 p (in Russian)

Lentz D (1992) Petrogenesis and geochemical composition of biotites in rare-element granitic pegmatites in the southwestern Grenville Province, Canada. Mineral Petrol 46: 239–256

Levillain C, Maurel P, Menil F (1981) Mössbauer studies of synthetic and natural micas on the polylithionite-siderophyllite join. Phys Chem Minerals 7: 71–76

Lewis HC (1880) On siderophyllite – a new mineral. Proc Acad Natural Sci Philadelphia 32: 254–255

Loucks RR (1991) The bound interlayer H_2O content of potassic white micas: muscovite hydromuscovite-hydropyrophyllite solutions. Am Mineral 76: 1563–1579

Lowell GR, Tobey EF (1979) Composition of an unusual zinnwaldite from southeastern Missouri. Mineral J 98: 445–459

Menzies MA, Boggs RC (1993) Minerals of the Sawtooth Batholith, Idaho. Mineral Rec 24: 185–202

Monier G, Robert JL (1986) Evolution of the miscibility gap between muscovite and biotite solid solutions with increasing lithium content: an experimental study in the system K_2O-Li_2O-MgO-FeO-Al_2O_3-SiO_2-H_2O-HF at 600 °C, 2 kbar P_{H_2O}: comparison with natural lithium micas. Mineral Mag 50: 641–651

Němec D (1983a) Zinnwaldit in moldanubischen Lithium-Pegmatiten. Chem Erde 42: 197–204

Němec D (1983b) Masutomilite in lithium pegmatites of West-Moravia, Czechoslovakia. N Jb Miner Mh: 537–540

Ponomareva NI, Gordiyenko VV (1991) Physico-chemical conditions of formation of lepidolite. Zap Vses Mineral Obshch 120: 31–39 (in Russian)

Ponomareva NI, Gordiyenko VV, Butorin VV (1993) Physico-chemical conditions of formation of lithium-ferrous iron micas in granitic pegmatites. Zap Vses Mineral Obshch 122: 102–106 (in Russian)

Puffer JH (1972) Iron-bearing minerals as indicators of intensive variables pertaining to granitic rocks from the Pegmatite Points area, Colorado. Am J Sci 272: 273–289

Rancourt DG, Dang MZ, Lalonde AE (1992) Mössbauer spectroscopy of tetrahedral Fe^{3+} in trioctahedral micas. Am Mineral 77: 34–43

Rieder M (1970) Chemical composition and physical properties of lithium-iron micas from the Krušné hory Mts (Erzgebirge) with chemical analyses by *M Huka, D Kučerová, L Minařík, J Obermajer* and *P Povondra*, part A. Chemical composition. Contrib Mineral Petrol 27: 131–158

Rieder M (1971) Stability and physical properties of synthetic lithium-iron micas. Am Mineral 56: 256–280

Robert JL, Volfinger M, Barrandon JN, Batsutcu M (1983) Lithium in the interlayer space of synthetic trioctahedral micas. Chem Geol 40: 337–351

Rossman GR (1984) Spectroscopy of micas. In: *Bailey SW* (ed) Reviews in mineralogy, vol 13. Min Soc of America, pp 145–181

Schärer U, Allegre CJ (1982) Uranium-lead system in fragments of a single zircon grain. Nature 295: 585–587

Simmons WB, Lee MT, Brewster RH (1987) Geochemistry and evolution of the South Platte granite-pegmatite system, Jefferson County, Colorado. Geochim Cosmochim Acta 51: 455–471

Stone M, Exley CS, George MC (1988) Compositions of trioctahedral micas in the Cornubian batholith. Mineral Mag 52: 175–192

Taylor MC, Foord EE (1993) Clay minerals associated with miarolitic rare-element pegmatites of the peninsular ranges batholith, southern California. Field Trip Guidebook for 30th annual meeting of the Clay Mineral Society, San Diego, CA, 31 pp

Wobus RA, Hutchinson RM (1988) Proterozoic plutons and pegmatites of the Pikes Peak Region, Colorado. In: *Holden GS* (ed) Geol Soc America Field Trip Guidebook 1988 (Prof Contrib of Colo School of Mines, no 12), pp 35–42

Author s addresses: *E. E. Foord*, M.S. 905, U.S. Geological Survey, Box 25046 DFC, Lakewood, CO 80225 USA; *P. Černý*, Department of Geological Sciences, Wallace Building, University of Manitoba, Winnipeg, Manitoba, Canada R3T 2N2; *L. L. Jackson*, M.S. 973, U.S. Geological Survey, Box 25046 DFC, Lakewood, CO 80225 USA; *D. M. Sherman*, M.S. 966, U.S. Geological Survey, Box 25046 DFC, Lakewood, Co 80225 USA; and *R. K. Eby*, Topometric, 1 Robertson Drive-Suite 18, Bedminister, NJ 07921-1716 USA